10 Orientation Growing from the Isotropic State

Straining of isotropic materials is a common method of testing or processing. During such treatment uniaxial orientation is frequently growing (Fig. 10.1).

Rigid Structural Entities. If the initial structure is described by rigid, anisotropic structural entities which are oriented at random, the evolution of anisotropic scattering is readily studied by means of the methods presented in Chap. 9. A practical example is the study of growing orientation in fiber-reinforced materials.

Shape Change of Structural Entities. In many cases the growing anisotropy is not only a phenomenon of rotating structural entities, but also goes along with a *deformation of the structural entities* themselves. This case will be studied here. Only affine deformations shall be discussed. In practice, such processes are observed while thermoplastic elastomers are subjected to mechanical load, but also while fibers are spun.

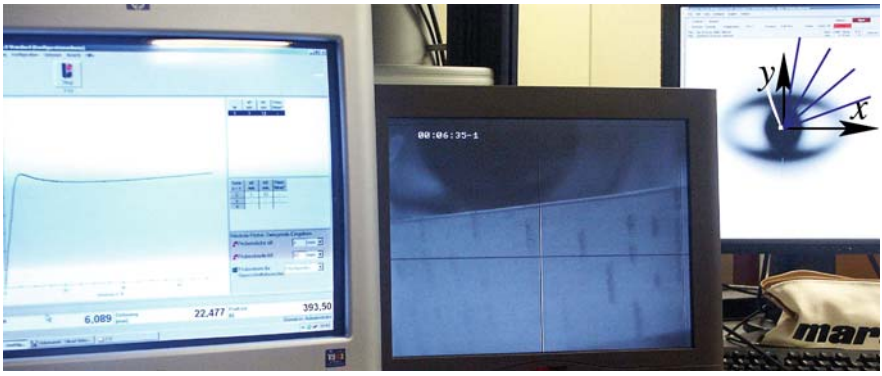

Figure 10.1. USAXS observation during straining of an SBS block copolymer. *Right monitor:* Intensity maxima on an ellipse. Raw-data coordinate system (x, y) and radial cuts for data analysis are indicated. *Middle:* Videotaping of sample. *Left:* Stress-strain curve. Control booth of beamline BW4, HASYLAB, Hamburg

The General Experimental Observation. Only the analysis of the most frequent experimental observation [248, 263–266] is discussed. In corresponding studies scattering curves are extracted in radial direction, and the positions of the found reflection maxima are plotted *vs.* the polar angle ψ' between the slicing direction and the fiber axis. As long as the material is isotropic, the reflection maxima are found on a spherical shell, the Debye sphere. As orientation is growing, the maxima are found on ellipsoidal shells, the ellipticity of which is increasing with increasing *draw ratio*, $\lambda_d = \varepsilon + 1$.

Evaluation Methods. Two evaluation methods are discussed in this chapter. RULAND's theory is based on reasoning concerning structure in 3D space. The strict approach relates structure to the scattering pattern. For example, the microscopic draw ratio of the structural entities can be determined. The other approach is the MGZ-technique of scattering image processing. Based on 2D master-peaks mapped by an elliptical transformation, almost any SAXS fiber pattern can readily be modeled. Long periods or tilt angles determined by the method are not more reasonably founded in scattering theory as are direct determinations from peak position and peak angle. Nevertheless, because the whole pattern is considered in the fit, small changes can be determined with higher significance. Thus the method is valuable for comparative studies. Moreover, it can be used to properly align raw patterns or to reconstruct patterns that are distorted – e.g., from accidental tilt of the specimen in the sample holder.

If the intended evaluation can be carried out on isotropic material, and thus the observed anisotropy is rather an obstacle than an advantage, the fiber pattern can be isotropized (cf. Sect. 8.4.2). This may, in particular, be helpful if lamellar structures are analyzed. If the focus of the study is on the anisotropic structure, the multidimensional CDF (cf. Sect. 8.5.5) may be a suitable tool for analysis. Several studies have demonstrated the power of the CDF method for the study of structure evolution during straining [174, 177, 181–183].

10.1 RULAND's Theory of Affine Deformation

10.1.1 Overview

In a fundamental paper [265] RULAND develops an advanced method for the analysis of scattering patterns showing moderate anisotropy. The deduction is based on a 3D model and the concept of highly oriented lattices. The addition of distortion terms makes sure that the theory is applicable to distorted structures and their scattering.

According to his deduction the common finding of ellipsoidal deformation of the reflections is indicative for affine deformation. Moreover, he arrives at an equation that permits to determine with high accuracy the microscopical draw ratio, λ_d, of the structural entities from the ellipticity of the deformed Debye sphere. This value can be compared to the macroscopical draw ratio. Even the intensity distribution along the ellipsoidal ridge is predicted for a bcc-lattice of spheres, and deviations of experimental data are discussed.

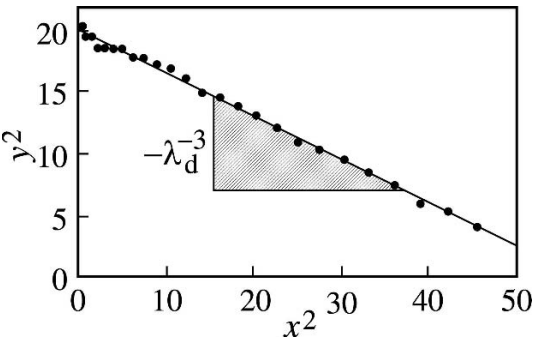

Figure 10.2. Plot of the positions (x,y) of peak maxima extracted on radial rays in a moderately oriented SAXS fiber pattern according to BRANDT & RULAND [265]. A microscopical draw ratio $\lambda_d = 1.41$ of the structural entities is determined from the slope

10.1.2 Application

Let (s_{12}, s_3) be the coordinates of reflection maxima determined on radial rays in the scattering pattern. Then a linearizing plot of the ellipsoidal shape is

$$s_3^2 = b^2 - \frac{b^2}{a^2} s_{12}^2, \tag{10.1}$$

with a and b being the semimajor and the semiminor axis of the rotation-ellipsoid, respectively. Then the equation [265]

$$\frac{b^2}{a^2} = \frac{1}{\lambda_d^3} \tag{10.2}$$

relates the slope in the linearizing plot from Eq. (10.1) to the microscopical draw ratio of the structural entities. The intercept

$$b^2 = \frac{1}{L_m^2} \tag{10.3}$$

in the linearizing plot is related to the extrapolated long period, L_m, in meridional direction (fiber axis). Figure 10.2 demonstrates the linearizing plot according to Eq. (10.1) for positions (x,y) of peak maxima extracted along radial rays from the 2D SAXS scattering pattern. x and y are in length units on the image (cf. Fig. 10.1). If $x = c\,s_{12}$ and $y = c\,s_3$ are valid, the draw ratio can be determined directly, without transformation from length units to the units of reciprocal space.

The clear linearity of the data demonstrates the affine character of the deformation. From the intercept, b^2, the semiminor axis of the rotation ellipsoid is determined. After transformation to units of reciprocal-space, the meridional long period follows from Eq. (10.3).

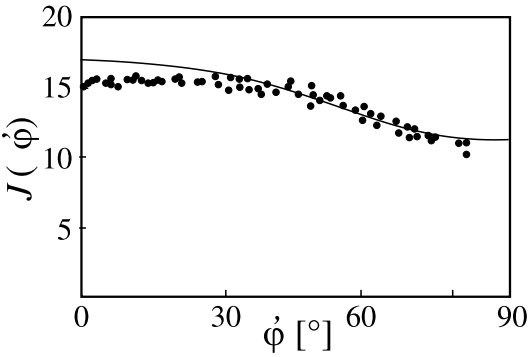

Figure 10.3. Shape of the maximum peak intensity, $J(\varphi')$, extracted from radial sections of a moderately anisotropic ($\lambda_d = 1.41$) SAXS pattern with fiber symmetry as a function of the sectioning angle φ' related to the fiber axis. *Dots:* experimental values. *Solid line:* Theoretical shape according to RULAND [265]

Modeling the initial structure by spherical domains in a bcc-lattice[1], the theoretical *intensity along the ellipsoidal ridge* as a function of the angle ψ' between fiber axis and the direction of the radial beam is

$$J_h\left(\varphi'\right) \propto g\left(\lambda_d, \varphi'\right) \left|\langle\Phi\rangle_D\right|^2 \left(s'_h\right) H_z^2\left(s'_h\right), \tag{10.4}$$

with

$$g\left(\lambda_d, \varphi'\right) = \frac{1}{\lambda_d}\sqrt{\frac{1+\lambda_d^{-3}\tan^2\varphi'}{1+\lambda_d^{-6}\tan^2\varphi'}}. \tag{10.5}$$

and

$$s'_h = s_h\sqrt{\frac{1}{\lambda_d}\sin^2\varphi' + \lambda_d^2\cos^2\varphi'}.$$

$\left|\langle\Phi\rangle_D\right|^2 \left(s'_h\right) H_z^2\left(s'_h\right)$ is the *form factor envelope*[2] of the scattering, made from the form factor of ideal spheres and the attenuation term describing a smooth transition of the density at the phase boundary (cf. p. 124).

The comparison between experimental and predicted intensity (Fig. 10.3) reveals deviations between theory and experimental data already at relatively low uniaxial deformation. A reasonable explanation is an increase of lattice distortions by local tensions which modify the envelope and thus the total intensity. Theoretical computation of mechanical anisotropy in a bcc-lattice supports the explanation [265].

[1] bcc: body-centered cubic arrangement of the spheres

[2] The form factor is, in fact, an envelope, because it limits the visibility of the reflections: Outside the region where it has decayed to virtually 0, no scattering is observed. Sometimes the envelope is visible: We "see" the spherical, the cylindrical or the layer shape of the fundamental domains in the oriented material.

10.2 The MGZ Technique of Elliptical Coordinates

Applicability. Just like RULAND in the previous section, MURTHY, GRUBB and ZERO [266–269], start from the common observation (Fig. 10.1). They propose a simple and powerful parameterization of scattering images of strained materials. Nevertheless, the method does not consider the 3D character (reflections on rotation ellipsoids, 3D structure model): movement of a peak from the meridian to the equator will decrease its observed "image-intensity", although such a decrease is – to a first approximation – a result of distributing the same intensity on a ring in space with a bigger diameter. Anyway, the intensity issue is not the focus of the MGZ method. Compared to the peak shape issue it is a more complex problem, as RULAND has shown (cf. p. 212).

Elliptical Coordinates. Scattering patterns can be expressed as a function of various coordinates. For isotropic scattering patterns, $I(\mathbf{s}) = I(s, \varphi, \psi)$, it is reasonable to choose polar coordinates, (s, φ, ψ), because the intensity is factorized $I(\mathbf{s}) = I(s)\, I_\varphi(\varphi)\, I_\psi(\psi)$ in these coordinates and two of the factors $I_\varphi(\varphi)\, I_\psi(\psi) = 1$ are constant.

Transferred to the observation that the reflections in moderately anisotropic scattering images are found on ellipses[3], it appears reasonable to parameterize such images in elliptical coordinates (u, v). The transformation relations are [266]

$$s_{12} = \sqrt{A^2 + u^2} \cos v \tag{10.6}$$

$$s_3 = u \sin v. \tag{10.7}$$

Here A is the distance of the foci, which are found on the s_{12}-axis. For $u = 0$ we have plane polar coordinates. Varying $v \in [0, 2\pi]$ at constant u describes an elliptical orbit with $a = \sqrt{A^2 + u^2}$ and $b = u$ its semimajor and semiminor axis, respectively.

If the elliptical parameterization shall be used for automatic alignment of scattering patterns, control of ellipse rotation and displacement are important. Rotation is controlled by subtraction of a constant from v. A displaced center is readily considered by subtraction on the left side of Eqs. (10.6) and (10.7).

Transferring RULAND's relation between the ellipticity and the microscopical draw ratio, λ_d, to the parameterization of MURTHY, GRUBB and ZERO, we receive

$$\frac{A^2}{u^2} = \lambda_d^3 - 1. \tag{10.8}$$

Figure 10.4 shows the first steps of scattering data analysis by means of of the MGZ technique. Replacing $\tan\phi = s_{12}/s_3$ in Eq. (10.1)

$$L_\phi^2 = L_M^2 + L_E^2 \tan^2\phi \tag{10.9}$$

is obtained. The equation describes the variation of the long period as a function of the polar angle, ϕ. The relations to the geometrical positions of the peak maximum in

[3] By not addressing scattering *patterns* and rotation-*ellipsoids* we stress the 2D character of the method.

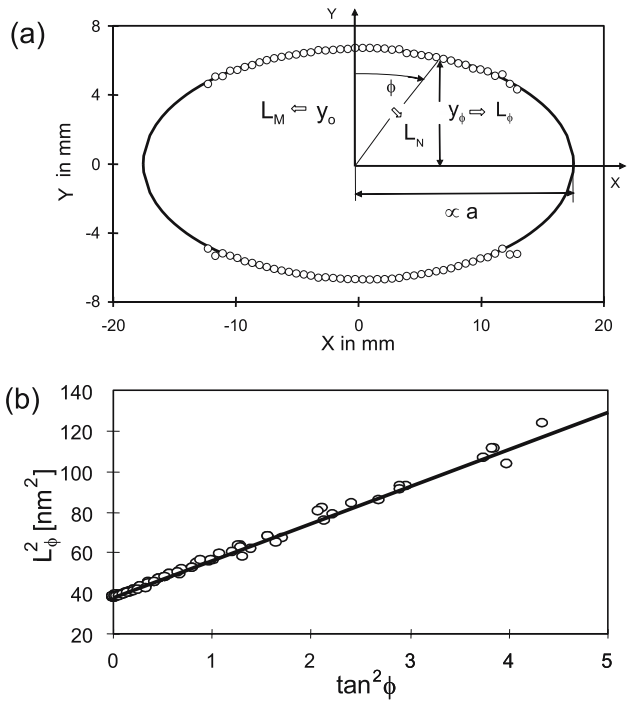

Figure 10.4. MGZ analysis of an undrawn polyamide 6 fiber. (a) Plot of the peak maximum position as a function of the detector coordinates (x,y). Relations to the parameters of the ellipse and the structure (long periods L_M, L_ϕ) are indicated. (b) Separation of meridional long period, L_M, from the long period L_ϕ. (courtesy S. MURTHY)

the scattering pattern are $L_\phi = 1/s_3$, $L_E = 1/a$, and $L_M = 1/b$. Here s_3 is not a variable, but the meridional component of the peak maximum expressed in units of the reciprocal space. The peak maxima are found on an ellipse with the semimajor axis a and the semiminor axis b. The validity of Eq. (10.9) to ϕ almost 90° is demonstrated in Fig. 10.4b using data obtained from an undrawn polyamide 6 fiber [269].

Parameterization of Reflections in Elliptical Coordinates. The authors of the technique define the intensity

$$I_j(u,v) = C_j f_j\left(u,u_{0,j},u_{w,j}\right) g_j\left(v,v_{o,j},v_{w,j}\right)$$

of the j-th model reflection by the product of two 1D functions, f_j and g_j, and a scaling factor C_j. $u_{0,j}$ and $v_{0,j}$ define the center of the reflection. $u_{w,j}$ and $v_{w,j}$ determine the breadths. A suitable class of functions for the 1D distributions is empirically found by study of the intensity curves in radial sections (cf. Fig 10.1) of the images. According to MURTHY, GRUBB and ZERO [266] a suitable class are Pearson-VII functions with shape factor $m = 2$.

Fiber symmetry makes that every function g_j is the sum of four quadrant functions,

$$g_j\left(v, v_{0,j}, v_{w,j}\right) = \frac{1}{4}\left(h_j\left(v, v_{0,j}, v_{w,j}\right) + h_j\left(v, \pi - v_{0,j}, v_{w,j}\right) + h_j\left(v, -v_{0,j}, v_{w,j}\right) + h_j\left(v, \pi + v_{0,j}, v_{w,j}\right)\right). \tag{10.10}$$

Thus every reflection in the fiber diagram is defined by one function $f_j\left(u, u_{0,j}, u_{w,j}\right)$ and four quadrant functions. If the model shall be fitted to a scattering pattern in which the fiber is tilted with respect to the primary beam, weighting factors are attached to each of the quadrant functions. After the fit of an experimental scattering image, the found factors quantify the tilt, and the corresponding distortion of the scattering pattern can be eliminated.